Visually Accurate Multi-Field Weather Visualization

Kirk Riley
Purdue University
kriley@ecn.purdue.edu

David Ebert
Purdue University
ebertd@purdue.edu

Charles Hansen
University of Utah
hansen@cs.utah.edu

Jason Levit
University of Oklahoma
jievit@ou.edu

Figure 1: Time Series of a Cloud Scale Visualization

Abstract

Weather visualization is a difficult problem because it comprises volumetric multi-field data and traditional surface-based approaches obscure details of the complex three-dimensional structure of cloud dynamics. Therefore, visually accurate volumetric multi-field visualization of storm scale and cloud scale data is needed to effectively and efficiently communicate vital information to weather forecasters, improving storm forecasting, atmospheric dynamics models, and weather spotter training.

We have developed a new approach to multi-field visualization that uses field specific, physically-based opacity, transmission, and lighting calculations per-field for the accurate visualization of storm and cloud scale weather data. Our approach extends traditional transfer function approaches to multi-field data and to volumetric illumination and scattering.

CR Categories: I.3.7 [Computer Graphics]: Three-Dimensional Graphics and Realism–color, shading, and texture

Keywords: Multi-Field Visualization, Visually Accurate Visualization, Weather Visualization

1 Introduction

One of the most common applications of visualization techniques is weather visualization. The majority of these images are created for representing weather data at the global, or synoptic, scale. At this scale, atmospheric interactions are approximately two-dimensional,

and involve global scale phenomena. Less commonly, but no less importantly, weather events are examined and predictions are made at the storm, or even cloud scale, where observation and visualization are particularly useful for the evaluation and prediction of severe storms.

Weather visualizations at the synoptic scale represent storms and fronts as they traverse the globe. At this scale, the data represents coarse scale quantities such as mean precipitation over large areas; therefore, visualization techniques conveying particular values are popular. Isosurfaces, and two-dimensional colored representations of weather fields convey particular data values to the observer. While these are effective when predicting large-scale weather patterns, they are ineffective when examining storm scale weather phenomena. Two-dimensional techniques cannot represent the highly three-dimensional event that is a forming severe storm. Although isosurfaces can represent exact data values in three-dimensions, they obscure the subtle details present in a storm.

We present a new visually accurate visualization system based on the particle scattering properties of the constituent fields. Through the use of these properties, we provide essential visual cues that are lost in standard weather representations. This new visually accurate weather visualization system improves the evaluation and prediction of cloud and storm behaviors from both simulation and measured weather data. This system may also be applied to cloud microphysics model evaluations and weather observer training.

2 Motivation

While representing particular data values with two-dimensional and isosurface coloring techniques in weather data sets is essential at the synoptic scale, it is often not the optimal approach to cloud and storm scale visualization. Meteorologists are trained to extract large amounts of information about a forming storm through observation in the field. Therefore, comprehension of storm scale data is maximized by presenting it in a visually accurate fashion. For example, a thunderstorm undergoes significant visual changes throughout its lifecycle, as it grows from a cumulus cloud, develops a cirrus anvil, and eventually develops rain, hail, and possibly severe weather. Rendering of numerical clouds to make convective clouds look "puffy," or cirrus clouds look "wispy," is important to help

279
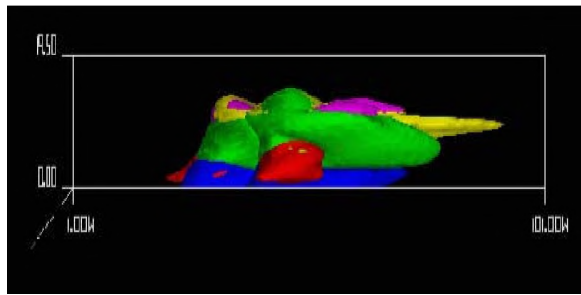
Figure 2: Isosurface Rendering of Storm Scale Data

rate interpretation of multi-field weather data based on the individual particle properties.

Volume rendering has been an important tool in rendering and visualization, starting with [Drebin et al. 1988]. [Ebert and Parent 1990] extended these techniques to gaseous volume rendering. [Engel et al. 2001] have concentrated on hardware accelerated volume rendering, while [Kniss et al. 2003] have focused on light transport models in volumetric systems. [Jensen and Christensen 1998] discuss realistic image generation with photon maps.

Procedural models have also been applied to rendering atmospheric phenomena. [Stam and Fiume 1995; Stam 1995] have discussed the modeling of gaseous phenomena with warped blobs, and the importance of diffusion in cloud rendering. [Ebert et al. 2003] describe many procedural techniques for cloud rendering.
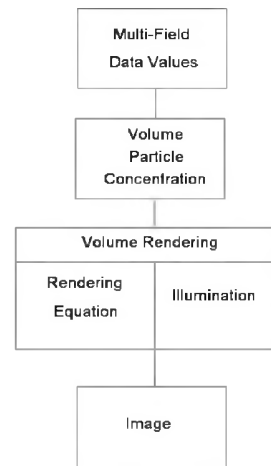
4 Visualization Methodology

Figure 3: Weather Visualization System Flow

a meteorologist determine the character of particular atmospheric features and structures. While isosurface methods can convey particular values of these multiple fields, they cannot represent the turbulent inhomogeneous mass of multiple-field weather. Inspection of a hard isosurface rendering of a severe storm from Vis5d [Hibbard and Sante 1986] in Figure 2 does not clearly communicate the structure of the storm because visual relationships among the various fields are obscured.

To achieve visual accuracy, we present a system based on the light scattering properties of the atmospheric particles. The various component particles in storms and clouds scatter light differently. Images that do not account for the different interactions of the particles with light do not provide believable visual cues to the observer. The scattering properties of these particles form the basis of the transfer function mapping from data values to the observed color and opacity.

Realistic weather visualization has many applications. Visually accurate representations will increase the effectiveness of storm scale atmospheric analysis and severe weather forecasting, improve the training of weather observers and students, and enhance the formulation, parameterizations, and physics of numerical weather prediction models.

3 Previous Work

Weather visualization has been an active area of research for many years [Papathomas et al. 1988; McCaslin et al. 2000; Trembilski 2002; Kniss et al. 2002]. One of the most widely used tools for weather visualization is the Vis5d system [Hibbard and Sante 1986]. Other important weather visualization systems are being developed by researchers at Georgia Tech [Tian-yue et al. 2001] and at IBM [Treinish 1997]. While these tools are useful in weather prediction and visualization, they do not provide visually accurate images needed for cloud scale and storm scale analysis.

Atmospheric rendering has also been an active research area, starting with the early low-albedo illumination model [Blinn 1982]. Extensions to this work in [Kajiya and Von Herzen 1984], showed the importance of multiple scattering in volumes. Unfortunately, fully realized multiple scattering systems are very computationally expensive. Advanced scattering and illumination methods have been developed [Max 1995; Klassen 1987; Nishita et al. 1996]. [Preetham et al. 1999] described an atmospheric scattering model for rendering daylight. A high-performance hardware accelerated forward scattering model, using impostors for the cloud rendering, and simulating cloud formation was presented in [Harris et al. 2003; Harris and Lastra 2001]. [Dobashi et al. 2002] developed atmospheric models for viewing the earth from space. While this research has developed techniques for rendering and illuminating atmospheric bodies, they do not provide a system for visually accu-

This system renders weather particle fields based on the particle properties. A diagram describing the structure of our rendering system is shown in Figure 3. To visualize these particles in an accurate manner, we first translate the input data fields into particle concentrations. We discuss meteorological data and how to translate it into particle concentrations in Section 4.1.

Volume rendering techniques allow us to represent a continuous field through transfer function mapping of data values to colors and opacities that correctly reveal the spatial relationships between thick, opaque structures and thin, wispy structures. Therefore, volumetric techniques are necessary to render multi-field data in a visually accurate manner. The volume model for weather data is presented in Section 4.2. Additionally, by visualizing the volume using the scattering of the individual particles, this system provides subtle visual cues crucial to understanding the composition of the storm as presented in Section 4.3 and Section 4.4.2.

Illumination is an essential cue for understanding the structure of three-dimensional storm fields. The high-albedo nature of cloud particles makes accurate illumination models difficult to apply at reasonable frame rates. Fortunately, phase function calculations show that large cloud particles heavily favor forward scattering, and hence a tractable translucency model [Kniss et al. 2003] is implemented. We present our illumination model in Section 4.4.

Storm models vary in their resolution and detail. Some applications of this system, such as the training of weather observers and

280

COMPUTER
SOCIETY

Variable	Definition
ρ_{air}	Density, $\frac{mass}{volume}$, of air $\frac{kg}{m^3}$
ρ_{field}	Density, $\frac{mass}{volume}$, of individual particles in field $\frac{kg}{m^3}$
volume$_{air}$	Volume of region of air under consideration m^3
η^{field}	Particle concentration, $\frac{particles_{field}}{volume}$
$T\left(\vec{s}, \vec{l}\right)$	Light attenuation between points $\vec{s}$ and $\vec{l}$
$L_l(\vec{s}, \Omega)$	Light contribution at point $\vec{s}$ in Ω direction
τ	Optical depth
β_{ex}	Extinction coefficient $\frac{1}{m}$
β_{ex}^{field}	Extinction coefficient for given field $\frac{1}{m}$
σ_{ex}^{field}	Extinction cross-section for given field $\frac{1}{m^2}$
$P(\Omega)$	Phase function
$CP(\Omega)$	Cumulative phase function
L_{lt}	Intensity of the light at source

Table 1: Variables List

even the evaluation of weather models, benefit from the capability for the user to introduce additional details. Therefore, we provide the user with the ability to add procedural details to storm and cloud scale weather visualization as described in Section 4.5.

4.1 Meteorological Data

A storm is comprised of many water particles of various states (ice/water), sizes, and habits (or shapes). Hydrometeor particles are the large (compared to air) water particles that create a storm cloud. The hydrometeor fields we currently consider in this model are cloud, ice, rain, snow, and graupel (soft hail). To properly render the multiple hydrometeor field data, we must determine how these particles interact with light. This relationship is dependent on the geometry of the particles and the concentration of those particles at a point in space. In this section, we focus on the issue of particle concentration.

Hydrometeor fields are often stored as mass ratios ($H_{field} = \frac{mass_{hydro}}{mass_{air}}$), where field specifies the hydrometeor field (cloud, rain, ice, snow, graupel, or vapor). In order to simplify our discussion, a list of variables is given in Table 1. An image showing the hydrometeor composition of a storm cloud is given in Figure 4. The color mapping is given in Table 2.
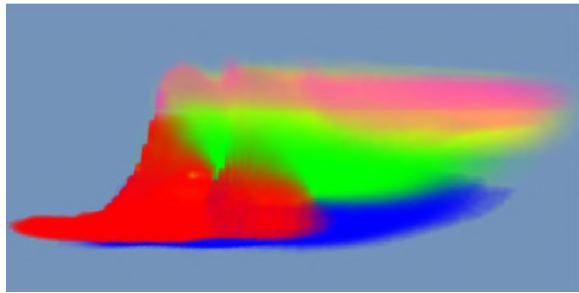

Figure 4: Cloud with Colored Hydrometeor Fields

Hydrometeor	Color
Cloud	Red
Ice	Magenta
Rain	Blue
Snow	Yellow
Graupel	Green

Table 2: Equivalent Spherical Particle Radii

Given the hydrometeor mass ratio and some properties of the particles, we determine the particle concentration. We define the particle concentration η^{field} as the particles per unit volume of that field. We assume the volume of air is much larger than the total volume of the particles. Therefore, the volume of the mixture is approximately the volume of the air. We calculate the total mass of all particles of a given particle field (tm$_{field}$) as the following:

$$tm_{field} = volume_{air}\rho_{air}H_{field} \qquad (1)$$

The total particles per volume is then expressed in terms of the mass of a single particle of that field, pm$_{field}$.

$$\eta^{field}volume_{air} = \frac{tm_{field}}{pm_{field}} \qquad (2)$$

pm$_{field}$ is defined as:

$$pm_{field} = volume_{particle}^{field}\rho_{field} \qquad (3)$$

The individual particle volume, volume$_{particle}^{field}$, is a function of the atmospheric conditions and the particle geometry of the given field. We now solve for the particle concentration of the given field.

$$\eta^{field} = \frac{\rho_{air}H_{field}}{volume_{particle}^{field}\rho_{field}} \qquad (4)$$

Now that we can translate the particle mass ratios into the concentrations of the various particles, we discuss the volume rendering model used in the system.

4.2 Volumetric Representation of Hydrometeor Particles

To properly render the various hydrometeor elements, a transfer function is applied to translate these ratios into opacities. Our volume rendering equation then determines the final color of each pixel, $L(\vec{w})$ using the following equation [Nishita et al. 1996]:

$$L(\vec{w}) = T(0, \vec{w})L_{bg} + \int_0^{\vec{w}} T(\vec{s}, \vec{w})\beta_{sca}(\vec{s})\int_{4\pi} P(\psi(\Omega))L_l(\vec{s}, \Omega)d\Omega d\vec{s} \qquad (5)$$

$T(\vec{s}, \vec{w})$ is the light attenuation between points $\vec{s}$ and $\vec{w}$. $\beta_{sca}(\vec{s})$ is the scattering coefficient. $P(\psi(\Omega))$ is the scattering phase function as a function of the angle between the incident light and the viewpoint, $\psi(\Omega)$. ψ equal to zero means the light is directly behind the viewpoint. L_{bg} is the background light intensity. $L_l(\vec{s}, \Omega)$ is the light at the point $\vec{s}$, in the direction Ω. Section 4.3 describes the calculation of $T(\vec{s}, \vec{w})$ for multi-field hydrometeor elements, and Section 4.4 discusses our translucency model used for calculation of $L_l(\vec{s}, \Omega)$.

281

Hydrometeor	Equivalent Radius mm
Cloud	0.01
Ice	1
Rain	1
Snow	2
Graupel	2.5

Table 3: Equivalent Spherical Particle Cross Sections

4.3 An Optical Model for Multiple Hydrometeor Fields

We now calculate the attenuation term of Equation 5 using the particle concentration calculated in Section 4.1. The intensity attenuation as we traverse the cloud, $T(\vec{s},\vec{w})$, for a given sample is often described in terms of the optical depth τ [Fu and Liou 1993; Blinn 1982; Nishita et al. 1996; Max 1995].

$$T(\vec{s},\vec{w}) = e^{-\tau} \qquad (6)$$

For an inhomogeneous volume, this optical depth is the integral of the extinction coefficient at that point in space with respect to distance.

$$T(\vec{s},\vec{w}) = e^{-\int_{\vec{s}}^{\vec{w}} \beta_{ex}(\vec{s}')\,d\vec{s}'} \qquad (7)$$

Numerically, we approximate the optical depth of a sample in terms of the extinction coefficients $\beta_{ex}^{field}(\vec{s})$ of the hydrometeor fields and the width of the sample Δs ([Key et al. 2002]).

$$\tau_{sample} \approx \left(\sum_{\text{All Fields}} \beta_{ex}^{field}(\vec{s}) \right) \Delta s \qquad (8)$$

Δs is the length of the current sample. The extinction coefficient for a given field β_{ex}^{field} is a function of the average particle extinction cross section for the given field (σ_{ex}^{field}) and the particle concentration of that field η^{field} [Nishita et al. 1996].

$$\beta_{ex}^{field} = \sigma_{ex}^{field} \eta^{field} \qquad (9)$$

For ice and clouds, we assume the single-scattering albedo to be approximately 1 [Key et al. 2002][Fu and Liou 1993]. Thus, by Equation 10 and Equation 11, the extinction cross-section is dominated by the scattering cross section.

$$Albedo = 1 - \frac{\sigma_{abs}}{\sigma_{ext}} \qquad (10)$$

$$\sigma_{ext} = \sigma_{abs} + \sigma_{sca} \qquad (11)$$

The scattering cross section, for hydrometeor particles substantially larger than the wavelength of light, is approximately twice the average geometric cross section [Liou et al. 1991; Bohren and Huffman 1983] of the particles. Cloud and rain particles are approximately spherical; therefore, the extinction cross section estimate for these particles is twice the area of a circle with radius equal to the particle radius. Although many hydrometeor particle shapes exist, particularly in ice fields [Key et al. 2002], we use an equivalent spherical cross section for all the particles. A table of approximate cross sections is given in Table 3 [Pruppacher and Klett 2000].

Rendering the various fields according to their combined extinction is essential to understanding the structure of the cloud in a visually accurate system. Comparing images with different β_{ex} for the various fields in Figure 6 and equal extinctions for all fields in Figure 5, we see a dramatic difference.

In summary, we have developed the calculation of the extinction for each of the fields β_{ex}^{field}. This enables the calculation of the
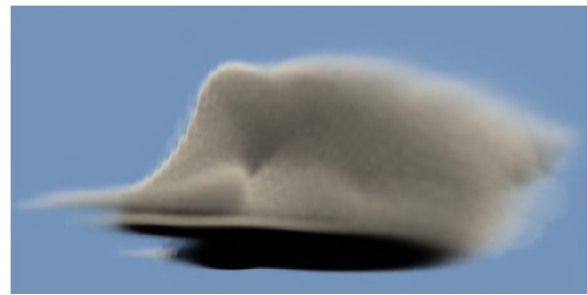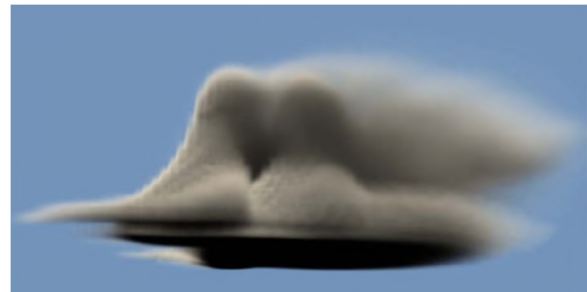

Figure 5: Improperly Scaled Hydrometeors Low-Albedo

Figure 6: Properly Scaled Hydrometeors Low-Albedo

overall optical depth by Equation 8, which is then used to calculate the overall attenuation factor $T(\vec{s}',\vec{w})$ in Equation 5. Now, with the attenuation coefficient available, we focus our attention on the model for $L_i(\vec{s}',\Omega)$.

4.4 A Physically Inspired Illumination Model for Cloud Rendering

In this model, there are two primary aspects of illumination. The first is the light transport model, i.e., how we calculate $L_l(s)$. The second is the overall phase function at s. We first describe our light transport approximation, then we discuss how we apply the phase function for the combination of hydrometeor fields.

4.4.1 Translucent Light Transport Model

Light transport calculations determine the extinction of light as the combination of absorption and outscattering of light, based on the absorption and scattering cross sections of the particles. Because of the high-albedo nature of clouds, the absorption cross section is negligible, but the outscattering is quite high. If we consider all the photons that strike a cloud particle as lost to outscattering (the low-albedo model [Blinn 1982]), we see in Figure 6 that the clouds become dark too quickly.

To account for multiple scattering we need to use an appropriate phase function model. If we consider one phase function model, the Cornette and Shanks model [Cornette and Shanks 1992], and its cumulative phase function shown in Figure 7, we see that forward scattering is overwhelmingly dominant in small cloud particles. In fact, 90 % of the light is scattered within about 10 degrees. Although the phase function varies from field to field, all particles are large compared to wavelength, and, therefore, scatter predominantly in the forward direction. Therefore, a model similar to the translucency model described in [Kniss et al. 2003] is appropriate for clouds. This model creates sampling slices with a normal

IEEE
COMPUTER
SOCIETY

halfway between the eye and light vectors, thus taking samples that are well conditioned to both the eye and light viewpoints. Two two-dimensional buffers are used, one for eye compositing, and one to store the attenuation of light. The eye-pass samples the light buffer through use of the render-to-texture OpenGL extension at the fragment level to determine correct lighting for the fragment.
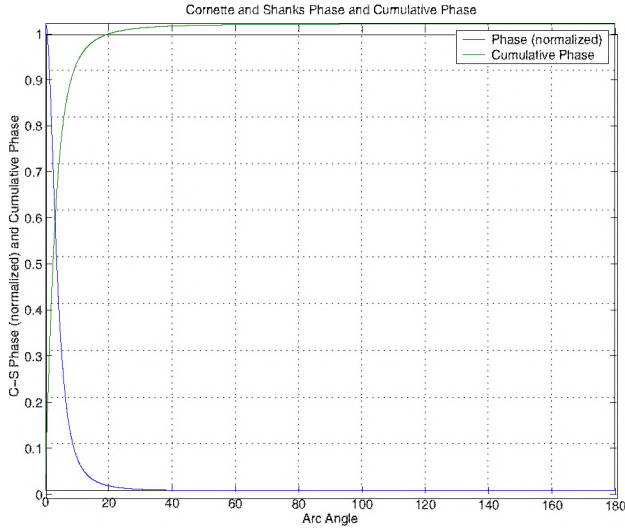

Figure 7: The Cornette and Shanks Phase (normalized) and Cumulative Phase for Clouds

Knowing that scattering in the cloud is predominantly forward scattering, we develop an approximation to calculate $L_l(\vec{s})$. For our illumination model, we break the light into three categories: unscattered light, forward scattered light, and outscattered (scattered in any non-forward direction) light. Unscattered light is the unimpeded light in the current sample. The forward scattered light consists of light that strikes a particle in the given region but still forward scatters. The outscattered light is the light that strikes the particle, scatters anywhere else, and is effectively extinguished. In our model, we define a forward scattering angle θ such that all light scattered within that arc towards the destination is considered forward scattered. This arc is shown for the per-pixel light buffer calculations in Figure 8. The light that contributes to the eye direction lighting as presented in Equation 5 is given in Equation 12 [Nishita et al. 1996].

$$L_l(\vec{s}, \Phi_{lt}) = L_{lt} T(\vec{s}, \vec{lt}) +$$
$$\int_{\vec{s}}^{\vec{lt}} T(\vec{s}', \vec{lt}) \beta_{sca}(\vec{s}') \int_{\theta} P(\Omega) L_l(\vec{s}', \Phi_{lt} + \Omega) d\Omega d\vec{s}' \quad (12)$$

The first term represents the unscattered light and the second term represents the contribution of light due to forward scattering over the θ arc angle, where L_{lt} is the intensity of the light source. Note that the assumption of high-albedo implies $\beta_{sca} = \beta_{ex}$. Despite the indirect peripheral contribution, we assume θ is small enough that $\psi(\Omega)$ is approximately constant over the arc. This allows us to factor the $P(\psi(\Omega))$ term in Equation 5, treating it as a directional light. For efficiency, we quantize this arc into two regions: a $\theta_f/4$ center region and a $\theta_f/4$ to $\theta_f/2$ outer region. We approximate the light in the center region as constant and equal to the center light contribution, and the light in the outer band as constant and equal to the average of four equally spaced samples around the band. In Figure 8, we show the calculation regions. The blue line represents unscattered light, the green lines the $\theta/4$ region, and the red lines
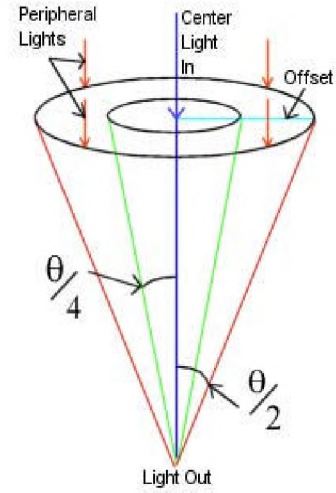

Figure 8: Per Pixel Calculation Regions for Translucency

the $\theta/2$ region. We are thus integrating the product of the phase and the light over a small forward angular region. The cumulative phase function, $CP(\theta)$, is the integral of the phase function. We calculate the light contribution to the light buffer in terms of this cumulative phase, the transparency in the center region, T_{ctr}, the transparency in the outer region, T_{per}, and the light contributions in the inner and outer arcs, L_{ctr}^{in} and $\overline{L_{per}}$.

$$CP(\theta) = \int_{\theta} P(\Omega) d\Omega \quad (13)$$

The unscattered propagating light is:

$$L_{unsc} = L_{ctr}^{in} T_{ctr} \quad (14)$$

The center region forward scattering is:

$$L_{forsc}^{ctr} = L_{ctr}^{in}(1 - T_{ctr}) CP\left(\frac{\theta_f}{4}\right) \quad (15)$$

The peripheral region forward scattering in terms of the mean peripheral light: $\overline{L_{per}}$ is then:

$$L_{forsc}^{per} = \overline{L_{per}}(1 - T_{per})\left[CP\left(\frac{\theta_f}{2}\right) - CP\left(\frac{\theta_f}{4}\right)\right] \quad (16)$$

Equations 15 and 16 combine to form the second term in Equation 12. The final light propagating to the next pixel is then given in Equation 17 below.

$$L_l(\vec{s}, \Phi_{lt}) = L_{unsc} + L_{forsc}^{ctr} + L_{forsc}^{per} \quad (17)$$

To maintain calculation tractability, we reduce volume texture reads by assuming that the extinction for center and for peripheral light is approximately the same: $T_{ctr} \approx T_{per}$. This equation is applied to the system using techniques similar to [Kniss et al. 2003]. An image with translucency illumination is given in Figure 9. Notice the softness caused by the blurring and the prevention of artificial low-albedo darkening in the cloud.

283

Figure 9: Cloud with Translucent Illumination

4.4.2 Particle Dependent Phase Functions

The scattering of a particle is largely dependent on its shape and size. As water particles increase in size, accurate particle scattering calculations change from a predominantly Rayleigh scattering model to a Mie scattering model [Bohren and Huffman 1983]. Mie scattering favors greater forward scattering as the particle size increases significantly above the wavelength of the light. Additionally, the scattering becomes less wavelength dependent. Examination of cloud water phase functions and ice water phase functions [Wendling et al. 1979] reveals that cloud water has higher forward scattering, while ice particles have more side and back scattering. To model this effect, we apply different phase functions to water (cloud and rain) and to ice fields (ice, snow, graupel). Phase is applied to the illumination of the system as given in Equation 12. These phase functions are based on the calculated values in Wendling, Wendling, and Weickman [Wendling et al. 1979]. Each phase function is calculated based on the relative concentration of each field, weighted by the field's extinction coefficient [Key et al. 2002].

$$\text{Phase}_{\text{voxel}}(\Theta) = \frac{\sum_{\text{AllFields}} \text{Phase}_{\text{field}}(\Theta) \beta_{\text{sca}}^{\text{field}}}{\sum_{\text{AllFields}} \beta_{\text{sca}}^{\text{field}}} \qquad (18)$$

Note that the dominance of forward scattering, and the limitations imposed by modeling the sunlight as an RGB color, requires the phase function to be normalized over its dynamic range and the peak at zero degrees truncated. A plot of the normalized phase functions used in this simulation is given in Figure 10. For comparison, a rendering of the system with particle based phase is given in Figure 11(b). Compared with Figure 11(a), we can see subtle differences between the ice fields in the center and top of the cloud, and the water fields to the outside and bottom of the cloud.

4.5 Procedural Detail for Visual Accuracy

Cloud and weather modeling systems are limited in their ability to cover all appropriate scales of detail. Large storm scale models (WRF, ARPS) effectively model the large structures of the cloud, but cannot calculate the behavior at smaller scales. Smaller cloud and microscale models can determine particle behavior, but cannot tractably model larger weather phenomena. Large phenomenological rendering can be enhanced by adding procedural details based on known cloud behavior to emphasize the different fields of the cloud. For example, we know that the cloud portion of a forming storm should be billowing, while the ice portion, as the cloud reaches the stratosphere, should be thin and wispy. Adding procedural details that differentiate fields based on these behaviors can be useful for model evaluation to determine what detail is missing, and to make more convincing images for the training of weather spotters. By multiplying a user adjustable portion of the data field
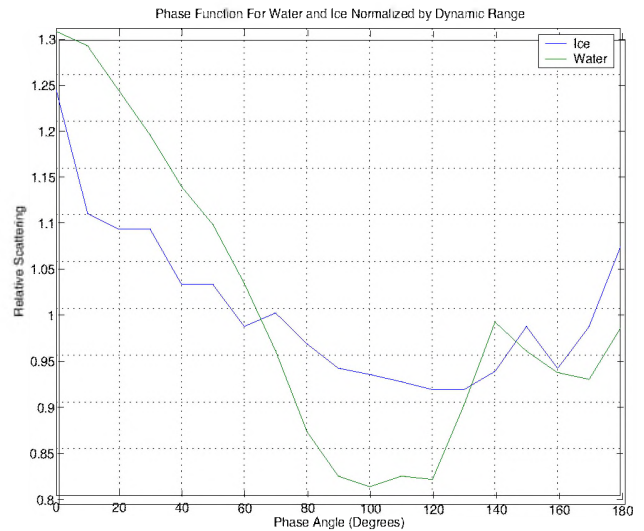

Figure 10: The Normalized by Dynamic Range Phase Functions for Ice and Water

Figure 11: Illumination with (a) Same Phase for All Particles and (b) Particle Specific Phase

with a Perlin noise texture [Perlin and Hoffert 1989], higher levels of detail are realized. Comparison of Figures 12 and 13 with Figure 4 shows how various noise levels in the different fields provide insight to the composition of the cloud. Figure 14 shows more natural viewing conditions of the storm simulation, where we are looking up at the storm cloud.

5 Results

For interactive visualization, it must be possible for the meteorologist to adjust the relative mixing ratios of the various fields at will. This system has been applied both to storm scale simulations, Figures 9, 11, 12, and to smaller cloud scale simulations, Figure 1. The storm level data was generated from the weather research and forecasting (WRF, http://www.wrf-model.org) model. This storm is approximately 20,000 meters tall and 100,000 meters long. This particular simulation is a splitting supercell storm. Through visually accurate visualization we determined, from the unrealistic smoothness of the cloud in the image, that the data generated from that simulation lacked medium scale turbulence that should have been present. The smaller cloud model represents a small cumulus cloud capable of light precipitation that is approximately 6500 meters tall and 6500 meters wide. It was created with a large-eddy simulation from the Straka Atmospheric Model [Straka and Anderson 1993], as modified in [Carpenter et al. 1998], and initialized with the parameters described in [Lasher Trapp et al. 2001]. Figure 1 shows

284

Figure 12: Large Scale Model with Additional Detail

Figure 13: Large Scale Model with Additional Detail

Figure 14: Bottom View of Large Scale Model with Additional Detail

three steps in the time series of the formation of a cumulus cloud.

To make adjustment of individual field (phase and extinction) properties available, without the need for costly recalculation of the data set, we use modern graphics hardware with per fragment calculation capability. The system presented here was implemented on an nVidia GeForceFX 5800 Ultra, using their Cg (C for graphics) compiler for vertex and fragment programs. Both the eye and light buffers require one vertex and one fragment program to evaluate Equations 5, 12 and 18 per fragment. This system provides great flexibility, but higher complexity options require highly complex fragment programs, which reduce performance. A table of the frame rates is given in Table 4 for a 300×300 image with 128 sampling planes (1 per voxel). Interactive rates are maintained for the less complex modes of the system, allowing the user to adjust settings in a fast mode, then examine the data with more advanced options.

6 Conclusions

We have developed a new visually accurate multi-field weather visualization system that effectively conveys fine volumetricly varying atmospheric data detail, improves the assessment of weather models, aids the training of weather observers, and presents more complete information in an intuitive style. Volumetric rendering

Mode	Frame Rate
Uniform Phase Low-Albedo Light	5.1 fps
Uniform Phase Translucent Light	4.28 fps
Per Field Phase, Translucent Light	1.68 fps
Per Field Phase, Noise Details, Translucent Light	1.18 fps

Table 4: Rendering Speeds (in frames/second) for various modes

systems are useful for weather data because of their capability to show varying degrees of opacity in inhomogeneous cloud systems. Our rendering system utilizes the individual extinction and scattering of these particles to produce a realistic representation that also provides insight into the structure of the cloud. Already, this system has been useful in determining missing turbulence components in one of the simulated models. These particle properties also reveal that forward scattering is dominant in hydrometeor particles, thus a translucency model is appropriate to the illumination of clouds. To improve differentiation and photorealism of cloud quantities, noise details can be added that provide additional cues to the user. Modern graphics hardware programs make flexible calculations possible at the fragment level, with varying costs in frame rate.

Acknowledgements

References

BLINN, J. 1982. Light reflection functions for simulation of clouds and dusty surfaces. *Computer Graphics 8*, 3 (July), 21–28.

BOHREN, C. F., AND HUFFMAN, D. R. 1983. *Absorption and Scattering of Light by Small Particles*. John Wiley and Sons.

CARPENTER, R. L. J., DROEGEMEIER, K. K., AND BLYTH, A. M. 1998. Entrainment and detrainment in numerically simulated cumulus congestus clouds, part i: General results. *J. Atmos. Sci. 55*, 3417–3432.

CORNETTE, W. M., AND SHANKS, J. G. 1992. Physically reasonable analytic expression for the single-scattering phase function. *Applied Optics 32*, 16 (June), 3152–3160.

DOBASHI, Y., YAMAMOTO, T., AND NISHITA, T. 2002. Interactive rendering of atmospheric scattering effects using graphics hardware. *Proc. Graphics Hardware*, 99–108.

DREBIN, R., CARPENTER, L., AND HANRAHAN, P. 1988. Volume rendering. *Computer Graphics (SIGGRAPH '88 Porc.) 22* (Aug.), 65–74.

EBERT, D. S., AND PARENT, R. E. 1990. Rendering and animation of gaseous phenomena by combining fast volume and scanline a-buffer techniques. *Computer Graphics 24*, 4 (Aug.), 357–366.

EBERT, D., MUSGRAVE, K., PEACHEY, D., PERLIN, K., AND WORLEY, S. 2003. *Texturing and Modeling A Procedural Approach*, 3 ed. Morgan Kaufman Publishers.

ENGEL, K., KRAUS, M., AND ERTL, T. 2001. High-quality pre-integrated volume rendering using hardware-accelerated pixel shading. *Proceedings of the ACM Siggraph/Eurographics Workshop on Graphics Hardware 2001*, 9–16.

FU, Q., AND LIOU, K. N. 1993. Parameterization of the radiative properties of cirrus clouds. *Journal of the Atmospheric Sciences 50*, 13, 2008–2025.

HARRIS, M. J., AND LASTRA, A. 2001. Real-time cloud rendering. *Eurographics 2001 Proceedings 20*, 3 (Sept.), 76–84.

HARRIS, M. J., BAXTER III, W. V., SCHEUERMANN, T., AND LASTRA, A. 2003. Simulation of cloud dynamics on graphics hardware. *Proceedings of Graphics Hardware 2003 (to appear)*.

HIBBARD, W., AND SANTE, D. 1986. 4-d display of meteorological data. *Proceedings of 1986 Workshop on Interactive 3D Graphics*, 129–134.

JENSEN, H., AND CHRISTENSEN, P. 1998. Efficient simulation of light transport in scenes with participating media using photon maps. *Proceedings SIGGRAPH '98, Computer Graphics Proc, Ann Conf Series*, 311–320.

KAJIYA, J. T., AND VON HERZEN, B. P. 1984. Ray tracing volume densities. *Computer Graphics 18*, 3 (July), 165–174.

KEY, J. R., YANG, P., BAUM, B. A., AND NASIRI, S. L. 2002. Parameterization of shortwave ice cloud optical properties for various particle habits. *Journal of Geophysical Research 107*, D13 (July), 4181.

KLASSEN, V. R. 1987. Modeling the effect of the atmosphere on light. *ACM Transactions on Graphics 6*, 3 (July), 215–237.

KNISS, J., HANSEN, C., GRENIER, M., AND ROBINSON, T. 2002. Volume rendering multivariate data to visualize meteorological simulations: A case study. *IEEE Visualization Symposium*, 189–194.

KNISS, J., PREMOZE, S., HANSEN, C., SHIRLEY, P., AND MCPHERSON, A. 2003. A model for volume lighting and modeling. *IEEE Transactions on Visualization and Computer Graphics 2003 9*, 2 (April-June), 109–116.

LASHER TRAPP, S., KNIGHT, C., AND STRAKA, J. 2001. Echoes from ultragiant aerosol in a cumulus congestus: Modeling and observations. *J. Atmos. Sci. 58*, 3545–3562.

LIOU, K., LEE, J., OU, S., FU, W., AND TAKANO, Y. 1991. Ice cloud microphysics, radiative transfer and large-scale cloud processes. *Meteorology and Atmospheric Physics 46*, 41–50.

MAX, N. 1995. Optical models for direct volume rendering. *IEEE Transactions on Visualization and Computer Graphics 1*, 2 (June), 99–108.

MCCASLIN, P. T., MCDONALD, P. A., AND SZOKE, E. J. 2000. 3d visualization development at NOAA forecast systems laboratory. *Computer Graphics 34*, 1 (Feb.), 41–44.

NISHITA, T., DOBASHI, Y., AND NAKAMAE, E. 1996. Display of clouds taking into account multiple anisotropica scattering and sky light. *Proceedings of the 23rd Annual Conference on Computer Graphics and Interactive Techniques*, 379–386.

PAPATHOMAS, T., SCHIAVONE, J., AND JULESZ, B. 1988. Applications of computer graphics to the visualization of meteorological phenomena. *Computer Graphics 22*, 4, 327–334.

PERLIN, K., AND HOFFERT, E. 1989. Hypertexture. *Computer Graphics 23*, 3 (July), 253–262.

PREETHAM, A. J., SHIRLEY, P., AND SMITS., B. E. 1999. A practical analytic model for daylight. In *Siggraph 1999, Computer Grahics Procedings*, Addison Wesley Longman, Los Angeles, A. Rockwood, Ed., ACM Siggraph, 91–100.

PRUPPACHER, H. R., AND KLETT, J. D. 2000. *Microphysics of Clouds and Precipitation*, 2 ed., vol. 18. Kluwer Academic Publishers.

STAM, J., AND FIUME, E. 1995. Depiction of fire and other gaseous phenomena using diffusion processes. *SIGGRAPH 95 Conference Proceedings, Annual Conference Series* (Aug.), 129–136.

STAM, J. 1995. Multiple scattering as a diffusion process. *Proceedings of the 6th Eurographics Workshop on Rendering, Dublin, Ireland* (June), 51–58.

STRAKA, J. M., AND ANDERSON, J. R. 1993. Numerical simulations of microburst-producing storms: Some results from storms observed during cohmex. *J. Atmos. Sci. 50*, 1329–1348.

TIAN-YUE, J., RIBARSKY, W., WASILEWSKI, T., FAUST, N., HANNIGAN, B., AND PARRY, M. 2001. Acquisition and display of real-time atmospheric data on terrain. *Eurographics-IEEE Visualization Symposium 2001*, 15–24.

TREINISH, L. A. 1997. Regional weather forecasting in the 1996 summer olympic games using an IBM SP2. *Proceedings of the AMS 13th IIPS* (Feb.).

TREMBILSKI, A. 2002. Transparency for polygon based cloud rendering. *Proceedings of the 2002 ACM Symposium on Applied Computing*, 785–790.

WENDLING, P., WENDLING, R., AND WEICKMAN, H. K. 1979. Scattering of solar radiation by hexagonal ice crystals. *Applied Optics 18*, 15 (Aug.), 2663–2671.

286

COMPUTER
SOCIETY